PV with multiple storage as function of geolocation to reduce peak demand

Giuseppe Colantuono, Ah-Lian Kor, Colin Pattinson, Chris Gorse

Leeds Sustainability Institute, Leeds Beckett University, LS1 3HE Leeds, UK

Abstract

A system, modeled in two geolocations (Oxford, England; San Diego, California), consists of a PV array and two storage solutions (defined by distinct sets of efficiencies/costs): short term (battery B) and long term (H, hydrogen reservoir with electrolyzer/fuel cell). The system meets a 1-year, real domestic demand totaling 5 MWh/year. First, it is configured as standalone (SA); then, as grid-connected (GC), receiving 50% of the yearly integrated demand. H and PV are dynamically sized as function of geolocation, B size and H efficiency.

With a 10 kWh battery and a 0.4 H cycle efficiency, required H capacity for the SA case is ∼1230 kWh in Oxford and ∼750 kWh in San Diego (respectively, ∼830 kWh and ∼600 kWh in the GC case). Related array sizes are, respectively, 93% and 51% of the local reference 8 kW$_\mathrm{p}$ system (51% and 28% in the GC case). A trade-off between PV size and battery capacity exists: the former grows significantly as B shrinks below 10 kWh. On the other hand, PV size is insensitive to rising B above ∼10 kWh, a capacity large enough to cope with short timescales.

With current PV and B costs, a SA system in Oxford (San Diego) can stay within 10^4 \$ CapEx if H's cost does not exceed 4 \$/kWh (8 \$/kWh); these figures increase to 7 \$/kWh (10 \$/kWh) with grid constantly/randomly supplying a half of yearly energy.

Extending modeling over 18 years makes results varying to different extents, depending on location; in any case, less than ±10% of the reference year.

Keywords: electricity storage, energy meteorology, solar energy, load following, power grid

1. Introduction

Non-constant output is a major obstacle towards a widespread exploitation of wind and solar photovoltaic (PV) generation, and a risk factor for the operational integrity of power distribution networks (Boyle, 2012; Steinke et al., 2013; Aghaei and Alizadeh, 2013). For this reason, energy storage is widely seen as the necessary addition to integrate large fractions of renewables in the power

grid, and to cope with demand drops caused by PV domestic installations' output during sunny days (Denholm et al., 2015). Storage on the users' side can also free the grid from the need of following demand. The price of batteries was still relatively high at the beginning of the 2010s (Mulder et al., 2013; Juul, 2012) but has then started to decline sharply; by some analysts (Hensley et al., 2012), this decreasing trend is projected to continue.

PV power is a typical example of highly inconstant renewable generation. Time-variability of solar irradiance on the Earth surface is due to two main astronomical facts, Earth rotation and revolution, which in turn correspond to separated timescales: day-night and seasonal cycles. The third source of irregularity is due to weather and climate, and is superimposed to the purely deterministic astronomical oscillations. It is often termed as intermittency in renewables literature and has a prominent effect on PV output, particularly in cloudy regions (see for example Colantuono et al., 2014a). Energy meteorology (Emeis, 2012; Kleissl, 2013; Olsson, 1994) is a growing field of research and testifies the importance of environmental analysis for maximizing renewables' output and quantifying/reducing uncertainty (Correia et al., 2017; Prasad et al., 2015; Colantuono et al., 2014b).

Storage coupled to PV power must therefore cope with these three sources of output variance. Other more or less unpredictable local factors that can further affect PV output range from module uncleanliness (Mani and Pillai, 2010), age-induced degradation (Kaplanis and Kaplani, 2011) and failure, to buildings obstructing the horizon (Erdélyi et al., 2014) and tree growth (Dereli et al., 2013). Domestic electricity demand is also affected by the discussed variability, as lighting and heating needs depend on season and weather patterns. All these environmental factors reach prominent importance when renewables supply a relevant fraction of electricity, because they affect both the generation and the demand side. PV is the only renewable source widely used on the domestic side, or for otherwise "small" applications ("microgeneration": typically, few kW_p, kWh of rated power, or less). From the distribution point of view, microgeneration reduces the customer's demand (before any residual is uploaded to the grid), while other renewables are integrated in the distribution network. The present model requires microgeneration be used locally: first, in a standalone (SA) configuration, and then in a grid-connected (GC) one.

Some authors (e.g. Zhou et al., 2011; Glavin et al., 2008, although with different aims and goals with respect to the present work) have suggested the coupling of different storage technologies to respond to different timescales. A few others, like for example Cau et al. (2014), couple hydrogen storage with batteries for SA systems/microgrids powered only by renewables, with the aim of finding an optimal energy management strategy. Here, we consider the same domestic load in two different geographical locations and climate. Firstly, demand is satisfied by PV (defined by the installed peak power) as the only power source, integrated with two coexisting storage reservoirs, schematized by their efficiency and cost: a long term hydrogen reservoir, H, coupled to electrolyzer and fuel cells, and a short term one, a lithium-ion battery, B. The sizes of the two reservoirs and of the PV array are dynamically determined for the chosen

locations by the requirement of matching the same domestic load's yearly time-series. PV size is expressed by means of the scaling factor X, the fraction of the size of an 8 kW$_\mathrm{p}$ array used as reference. The partition of storage into a long-term reservoir and a short-term, more efficient and smaller one is justified if a trade-off between storage cost and conversion inefficiency is possible.

Current storage technologies possess various efficiency levels; here, hydrogen H and battery B are characterized by their round-trip efficiency values η_H and η_B. H efficiency is given three values: $\eta_H = 30\%$, 40% and 50%, a range similar to what reported in Luo et al. (2015, Table 11 therein), while the battery efficiency is fixed at $\eta_B = 85\%$ (*ibid.*). The latter value can fall either within the lithium-ion (Rastler, 2010) or the Lead-acid (Beaudin et al., 2010) efficiency interval. The smallest η_H value is the closest to the currently available electrolysis/fuel-cell cycle; significant improvements may be expected with standardization and mass production, as hydrogen storage is still in the development phase (Luo et al., 2015).

PV generation is then supplemented by a power grid able to provide only constant power. This scenario is aimed at exploring storage as a substitute of the current load-following pattern (e.g. Moshövel et al., 2015); the amount of long- and short-term storage needed on the user's side to accommodate such a constant supply is quantified. This idea is further extended that a partly random power provision is fed by utilities to domestic customers, to understand how user's storage may cope with a grid that, besides not following demand, does not mitigate the variability on the supply side induced, for example, by wind and solar farms.

The two compared geographical locations are Oxford in the South of Great Britain and San Diego in Southern California. PV output and states of charge of the storage reservoirs are expressed as function of time in the two geolocations; PV arrays' sizes and reservoirs' capacities are determined in each location for a number of system configurations. Engineering implementation is beyond the scope of this analysis, the focus of which is energy balance. Exactly matching storage to given yearly demand and PV generation timeseries is not sufficient to size a real system, due to year-to-year variability. Further analysis is therefore performed to understand the behavior over many years, with the resulting variations of required generation and storage capacity.

2. Modeling the system

2.1. Generalities

The examined system comprises a 1 year-long domestic load from central France (Lichman, 2013) where the climate, loosely speaking, is somehow intermediate between the analyzed locations. Storage is divided into two reservoirs: a costly and efficient short-term storage B and an inexpensive and inefficient long-term storage H. Load is normalized to set its yearly integrated value to 5 MWh. PV generation needs to be standardized accordingly: its yearly integrated value in both locations must equal 5 MWh to match demand *after the*

losses due to storage round-trip conversions are taken into account. This implies that changing B reservoir's size makes PV array's area and H's capacity changing as well. Further case studies include power provision from the electric grid in the amount of 50% of the yearly-integrated demand, with PV array's size reduced accordingly.

Table 1: Main symbols

Symbol	Definition
$\mathcal{S}\,()$	Heaviside's step function
$T = 1$ yr	Length of the problem in time
$0 \equiv t_0, t_1, ... t_n, ..., t_N \equiv T/t_1$	60 s time-steps; $N = T/60s \equiv 525600$
d^B	Power drawn from battery
d^H	Power from H to battery
u^B	Power fed to battery
u^H	Power fed to H
λ	Electric power load in kW
γ	PV power generation
δ	Difference between generation and demand
X	Fraction of the reference, 8 kW$_\mathrm{p}$ PV array
B	Battery (and its state of charge)
H	Hydrogen storage (and its state of charge)
η_H	Energy efficiency of long term storage (H)
η_B	Efficiency of short term storage (battery)
B_m	Minimum battery charge level
B_M	Battery capacity

A system with no battery (endowed with H only) has not been considered due to the relatively slow start-up time of fuel cells. Battery is never discharged below $X \cdot \max(\lambda) * 600$ s$= 0.91 \cdot X$ kWh, where X is the PV array scale factor in terms of percentage of the reference, 8 kW$_\mathrm{p}$ array; a 600 s interval is of the order of H's reservoir latency. Such a buffer should ensure power shortage avoidance; it also causes effective B capacity to be lower than labeled. In a real system, an additional small penalty, neglected here, would be present, because a fraction of the power drawn from H would be routed through B in transient phases, between the time H kicks-in until it reaches working conditions. The number of such transients would be relatively small, as H tends to be switched on/off with a much lower frequency with respect to battery.

2.2. Governing equations

We are aimed at determining storage reservoirs' states of charge $B(t_n)$ and $H(t_n)$ as function of previous states $B(t_{n-1})$ and $H(t_{n-1})$ and of generation $X\gamma$ and load λ. X needs to be determined as well. Time dependency is

henceforth omitted to simplify notation, barring cases where functions depend on previous time step t_{n-1}.

We first define δ, the difference between generation and load at any time t_n:

$$\delta = X \cdot \gamma - \lambda; \tag{1}$$

X scales the generation timeseries γ to adapt PV array's nominal power to system's features as they are varied throughout the model's scenarios.

We then label uploaded and downloaded power as u^X and d^X. Consequently, the non-negative variables u^B and u^H quantify the power uploaded to battery B and to long-term reservoir H, respectively:

$$u^B = \mathcal{S}[\, B_M - \eta_B \delta - B(t_{n-1})] \cdot \mathcal{S}(\delta) \cdot \delta +$$
$$+ \, \mathcal{S}\big\{ -[\, B_M - \eta_B \delta - B(t_{n-1})] \big\} \cdot [B_M - B(t_{n-1})]\,/\eta_B \,, \tag{2}$$
$$u^H = \mathcal{S}\big\{ -[\, B_M - \eta_B \delta - B(t_{n-1})] \big\} \cdot \big\{ \delta + [B(t_{n-1}) - B_M]\,/\eta_B \big\}; \tag{3}$$

symbols are detailed in Table 1, while

$$\mathcal{S}(x) = \begin{cases} 1, & \text{if } x > 0; \\ 0, & \text{otherwise} \end{cases}$$

is the Heaviside's step function according to the $\mathcal{S}(0)=0$ convention (brackets of any kind following $\mathcal{S}$ always denote its functional argument). This function plays the role of a switch, defining the system's regime: for example, when δ changes from positive to negative, the quantity $\mathcal{S}(\delta)$ goes from 1 to zero, setting the first term of Eq. (2) to zero. This is all the more so for the second term (and for the right-hand side of Eq. 3 as well), because $\delta \leq 0$ implies $\eta_B \cdot \delta + B(t_{n-1}) - B_M \leq 0$.

Battery is being charged ($u^B > 0$) when both generation is larger than λ (that is, $\delta > 0$) and B is not full; if either condition is not met, $u^B = 0$ holds instead. On the other hand, long-term storage H is being charged ($u^H > 0$) when $\delta > 0$ and B is completely filled up; that is, the relationships $B(t_n - 1) = B_M$ and $X \cdot \gamma > \lambda$ are true at the same time. The first term of Eq. (2) represents the case in which the 60 s "energy packet" to be loaded at the current time-step does not saturate the capacity of the battery when added to the energy already in it. The second term refers to the incoming packet saturating the battery, in which case the packet can only be partially taken up. In the latter instance, the energy uploaded to B corresponds to the difference between capacity B_M and $B(t_n - 1)$, the level of charge resulting from balance at previous time-step. The energy needed to fill such a capacity is the capacity itself divided by B's efficiency $\eta_B < 1$; this takes into account round-trip storage losses, for simplicity attributed entirely to the uploading phase. The only term on the right-hand side of Eq. (3) "completes" the action of the second term of Eq. (2): the fraction of the incoming energy packet that does not fit in B (or the entire packet, if $B(t_{n-1}) = B_M$) is uploaded to H instead.

Power downloaded *from* reservoirs is instead denoted by the non-negative functions d^B and d^H:

$$d^B = -\mathcal{S}(-\delta) \cdot \delta; \tag{4}$$

$$d^H = -\mathcal{S}(-\delta) \cdot \mathcal{S}[B_m - B(t_{n-1})] \cdot \delta; \tag{5}$$

that is, the common, necessary condition for d^B and d^H to differ from zero is $X \cdot \gamma < \lambda$. d^B also needs to satisfy $B_m \leq B(t_{n-1}) \leq B_M$ (the Heaviside's condition expressing the latter inequality is automatically satisfied and therefore absent from Eq. 5); d^H must meet $B(t_{n-1}) < B_m$ instead.

The drop of battery level below the threshold value B_m is the event that triggers H's discharge (Eq. 5): as soon as the quantity $B_m - B(t_{n-1})$ becomes greater than zero, H starts to provide an amount of energy equal to $|\delta|$ that, added to generation, satisfies demand. Battery level is restored at $B = B_m$ or higher as soon as δ becomes greater than zero. Until that occurs, H remains active; that is, d^H remains above zero.

We can finally quantify the energy level in both B and H reservoirs:

$$B = \mathcal{S}(t_2 - t_n) \cdot B_M + \mathcal{S}(t_n - t_1) \cdot \left\{ B(t_{n-1}) + \eta_B u^B + d^H - d^B \right\}; \tag{6}$$

$$H = \mathcal{S}(t_2 - t_n) \cdot H(0) + \mathcal{S}(t_n - t_1) \cdot \left[H(t_{n-1}) + \eta_H u^H - d^H \right]; \tag{7}$$

Heaviside's conditions, in this case, separate reservoirs' initial energy level ($t_n = 1$) from the evolution that follows ($t_n > 1$).

In summary, both B and H depend on load λ and generation $X\gamma$ via δ through Eqs. (2-4); B and H also depend on time, on the fixed parameters B_m, B_M, η_B, η_H, and on their prior states. Examples of the behavior of the seven variables defined by Eqs. (1-7) are displayed in Appendix B.

The energy in the d^H term is recorded as "in transit" through the battery (penultimate monomial in Eq. 6) to stress that it is battery's sub-threshold level that triggers and keeps H's discharging. However, d^H is thought to bypass B and satisfy demand without any intervening stage (keeping in mind what discussed on H's transients at bottom of Section 2.1): the η_B energy penalty is therefore not assigned to d^H. Real-world systems could clearly be tweaked with different criteria; the implementations of these range of conditions will be use cases. The present implementation, which minimizes the required PV array size by using the less efficient, long-term reservoir only when battery is full, has the advantage of not requiring any kind of online computation.

The last equation needed to close the problem is given by the constraint

$$H(T) + B(T) = H(0) + B_M. \tag{8}$$

The requirement that the amount of long-term stored power at the end of the yearly period equals the initial level (system is set to start with a full battery, implying $B(0) \equiv B_M$ in Eq. 8) assures that yearly-integrated generation and load are equal as well, once all conversion's inefficiencies have been taken into account. In order to find a practical, approximate solution, the equality in

Eq. (8) will be considered satisfied if the two sides differ less than a predetermined amount ("error").

Once B's capacity is fixed and both H and the PV array are sized accordingly, the historical data (past generation and demand timeseries) will not be necessary for operating a real system. The approach here is aimed at highlighting geographical/climate differences, and the behavior induced by various battery sizes. The sizing of a real system would have to account, for example, for year-to-year differences in solar generation and electricity consumption, failure rate, and other unpredictable factors; consequently, some form of uncertainty evaluation should be introduced, e.g. loss-of-load probability (LOLP, discussed by Celik, 2007; Klein and Beckman, 1987; Schenk et al., 1984, and many others). The impact of differences in PV generation over many years is addressed in Section 5, as well as the effect of varying demand. LOLP estimation is not addressed here, as it would not make substantial contribution to frame the problem of multiple storage as function of climate and geolocation.

2.3. Solution of Eqs (1-8)

Equations are solved for every time t_n as function of previous time t_{n-1}, for a guessed value of X; the procedure is being iterated until "error" falls below a predetermined threshold. H at $t = 0$ contains an amount of energy equal to 2 months of the yearly integrated load: $H(0) = (5/6)$ MWh (the used datasets are detailed in the next section). The first step (from 00:00 to 00:01, January 1) simply updates battery storage, which is being depleted by 60 s worth of load as PV generation is zero at nighttime. As time advances, the appropriate Heaviside's functions will transit from zero to 1 and vice versa. B becomes progressively depleted, but the Sun later kicks in. B may therefore be recharged or, if generation is insufficient, may fall below the minimum level B_m, in which case H will start to feed the demand instead. At the end of the yearly timeseries, the final value $H(T) + B(T)$ is recorded.

For the sake of computing a practical solution, Eq.(8) is replaced by the following approximate condition, as anticipated above:

$$| H(T) + B(T) - H(0) - B_M | < 10 \text{ kWh}. \tag{9}$$

If Eq. (9) is not satisfied and the argument of the absolute value on the left-hand side is negative, the size of the PV array is increased by increasing X; if, on the contrary, such an argument is positive, X will be reduced. After this update the procedure is repeated and H updated again. The process is interrupted as soon as the condition in Eq. (9) is met. Capacity of long-term storage H is defined as

$$\overline{H} = \max [H(t_n)] - \min [H(t_n)] . \tag{10}$$

The 10 kWh allowed maximum difference (error) between initial and final H value is here considered negligible with respect to the 5 MWh yearly integrated load. The model allows to arbitrarily reduce the error, at expense of computational speed. From a coding point of view, a "while loop" is being employed to

keep the model running and the iterations following one another until an appropriate PV array's size is found and the inequality at Eq. (9) satisfied. When this occurs, yearly generation balances the yearly demand, storage's round-trip penalties included.

2.4. Demand and Generation data

A domestic consumption timeseries and a PV generation one are needed in each geolocation in order to address the formulated problem. the same domestic-load timeseries (Lichman, 2013) is used in both localities: Oxford, UK (hereafter Oxford, Oxford PV array 2016) and San Diego, CA, USA (hereafter San Diego, PVOutput.org 2017b). This choice has the downside of neglecting the local correlation between PV generation and household power demand (e.g., on a sunnier-than-average day, lower lighting demand may be expected, together with relatively high PV output) but has the big advantage of comparing the performance of both generation and storage in different locations against *the same* demand curve, which is the main goal of this study. With the loss of co-spatiality between generation and demand, contemporaneity loses its meaning, too: timeseries have been therefore chosen to prioritize availability and data integrity.

The load λ is normalized to 5 MWh of yearly generation, which cuts approximately by a half the original load's size. This integrated value is considerably lower than the average electrified USA home ($\sim$ 12300 kWh in 2014, Energy Efficiency Indicators 2016) but higher than the yearly consumption of the average electrified home in the European Union in the same year ($\sim$ 3600 kWh, *ibid.*) and in China ($\sim$ 1600 kWh).

As already specified, the PV scaling factor X expresses the size of the needed PV array as a fraction of the reference 8 kW$_p$ PV array. The PV size needed in San Diego to achieve Oxford's output is 61% of Oxford's array, for the yearly timeseries used (Appendix A). This clearly introduces a dependency on the particular year considered when comparing the two geolocations. In Section 5, 18-year long records are considered, to overcome this limitation and to determine a range of variability for the model's quantities in both places. The size of PV arrays is expressed in kW$_p$, to keep our conclusions with the highest possible independence on the technology used. The two arrays have diverse orientations; none of the azimuths is due south (see Appendix A), meaning that the two PV arrays are surely sub-optimal. This does not diminish the significance of the present analysis because climate differences are overwhelming and the differences induced by systems' configuration (battery size, H efficiency, grid supply) are assessed by comparing results locally. Last but not least, orientation is rarely optimal for real, domestic PV arrays (usually constrained by the existing built environment, Colantuono et al. 2014a) and often known/reported by the owner with significant approximation (*ibid.*).

More information on the used timeseries can be found in Appendix A.

8

3. Results

3.1. Standalone systems

Standalone systems are useful analysis targets not only per se; they can be viewed as the limiting case for grid-connected (GC) systems, with microgeneration and storage, as grid-supplied electricity is progressively reduced. Eqs. (6-8) are solved for B, H, and X thirty times for each location, in order to combine three values of η_H (0.3, 0.4, 0.5) with ten values of battery size (2 to 20 kWh with 2 kWh increment). Solutions are sought by dynamically adjusting X such that $X \cdot \gamma$ satisfies the demand λ (Lichman, 2013) for the chosen battery size within the specified, 10 kW$_p$ error.
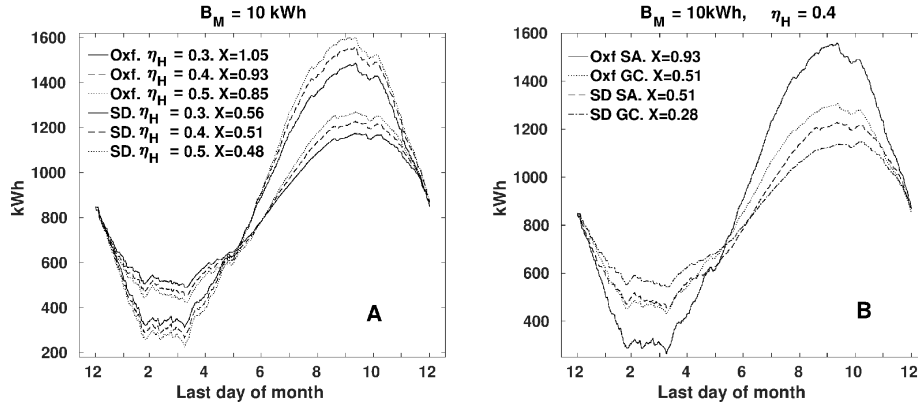

Figure 1: Panel **A**. Curves represent long-term storage H throughout the year. H's round-trip efficiency η_H (the second field in the legend, after geolocation) is being parametrically varied. The third field represents X, the PV array scaling factor; a similar scaling coefficient applies if PV's area is considered instead of peak power, provided technology is the same for all systems. The high degree of similarity at large-scale, between curves representing very different battery sizes in the same geolocation, may be misleading; a zoom on small scales features of the curves (Fig. 4) shoes the small-scales differences between systems with large and small batteries. Oxford's and San Diego's bunches of curves are well separated; they can be represented with the same line styles. H's curves in Oxford (San Diego) boast higher (lower) maxima and lower (higher) minima: more energy must be stored in Spring/Summer (Summer from now on) to be used in Fall/Winter (hereafter Winter) in more poleward latitudes. Battery has capacity $B_M = 10$ kWh. Panel **B**. Standalone (SA) systems compared to grid-connected (GC) ones, supplied with constant power summing up to 50% of integrated yearly demand, for the intermediate $\eta_H = 0.4$ value. GC case with 25% of random-varying power is not plotted as virtually indistinguishable from the constant-power case. Required long-term storage capacity in Oxford (San Diego) falls from ∼1230 KWh to ∼830 KWh (∼750 KWh to ∼600 KWh) with constant grid supply; capacities are the same for GC case with random-component).

In Fig. 1A the effect of hydrogen conversion efficiency in the chosen geolocations is shown. The difference between the maximum and the minimum amount of energy contained in long-term storage defines the required H capacity. The chosen demand can be satisfied by the San Diego PV array (of the specified orientation, see Appendix A) with size between 48% and 56% of the 8 kW$_p$ reference installed power, for a power-to-hydrogen round-trip conversion

efficiency η_H between 30% and 50% and a 10 kW$_p$ battery. The same conditions in Oxford require an array ranging from 85% to 105% of the 8 kW$_p$ reference power. The required PV size decreases with increasing η_H because a more efficient H storage reduces conversion losses and, consequently, the generation which is required to match demand. On the other hand, the required H capacity grows as a smaller PV array increases the need of storing energy from Spring/Summer (Summer from now on) to Fall/Winter (Winter from now on). In other terms, with a larger PV array and a less efficient seasonal storage H, more power is proportionally wasted in Summer to load the hydrogen reservoir (it is useful to recall that round-trip inefficiencies are here computed at once when energy is uploaded to reservoirs) but less energy is actually uploaded, as the larger array is closer to self-sufficiency in winter. Unlike Fig. 1A, where
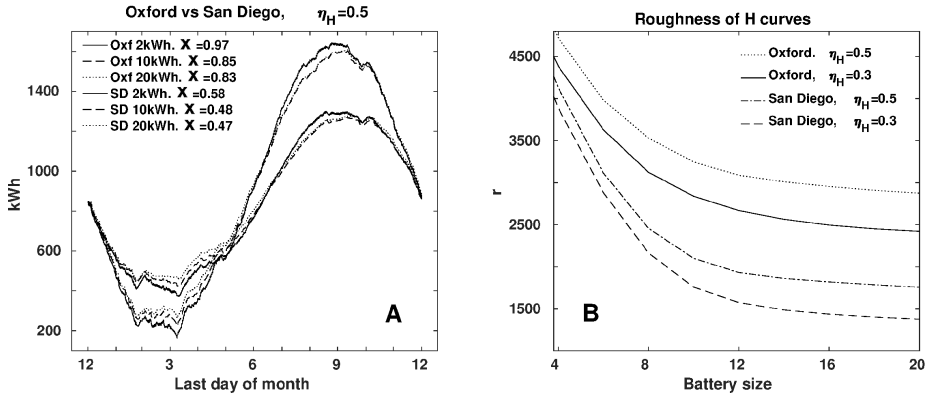

Figure 2: Panel **A**. Like Fig. 1A, with battery capacity being parametrically varied. As in Fig. 1A, the three San Diego curves reflect a much lower seasonal variability and are well separated from Oxford's ones. Legend's fields indicate geolocation, B capacity and PV array's *scaling factor* X; such a value needs to be multiplied by 8 kW$_p$, the array's reference size. Long-term storage round-trip conversion efficiency is here set to $\eta_H = 0.5$, the highest value. Panel **B**. Systems are compared from an alternative point of view, which highlights the different usage of long-term storage when geolocation and η_H are varied: "roughness" r (Eq. 11) is depicted. Higher r values indicate higher reliance on H and a "rough" H's profile (Fig. 4): the long-term reservoir's usage is proportionally higher on short timescales. r is inversely related to battery size, and is higher in the poleward location.

curves depict diverse η_H values, Fig. 2A's curves represent battery size once the most efficient hydrogen conversion efficiency has been picked ($\eta_H = 0.5$). The 10 kWh curve is virtually identical to the 20 kWh one, both in Britain and in California. This highlights that, for the given yearly demand curve, increasing battery size from $B = 10$ kWh to $B = 20$ kWh offers only marginal improvement as also testified by the associated small reduction of PV array size. On the other hand, the difference between the PV size required for a 10 kWh and a 2 kWh battery is significant because, when B is too small, the system is forced to rely on relatively inefficient H storage for hourly and daily transactions which occur with high frequency, from hundreds to a few thousands of times per year, compared to the few cycles per year (1 or 2) involved in seasonal storage. The

difference in the PV array size required by $B = 2$ kWh and $B \geq 10$ kWh suggests that the separation between long-term (seasonal) and short-term (daily-hourly) storage arises in a seamless and "natural" way when battery is large enough. No energy-management algorithm is required to direct power to the appropriate reservoir: the simple rule of first filling B up to capacity, and only subsequently converting electricity to hydrogen and loading the H reservoir, has the property of minimizing conversion inefficiencies and therefore minimizing the PV area required to feed the system.

The impact of battery size on PV size is further clarified by Fig. 3 (which also shows the similar effect battery size has on required H capacity): in both locations, for the same demand timeseries totaling 5 MWh per year, the 10 kW$_\mathrm{p}$ value can be loosely seen as the boundary between a capacity range ($B \lesssim 10$ kWh) characterized by a relatively strong dependency between battery capacity and PV size, and a range ($B \gtrsim 10$ kWh) where such a dependency is noticeably weaker as added battery capacity improves system's efficiency only marginally.
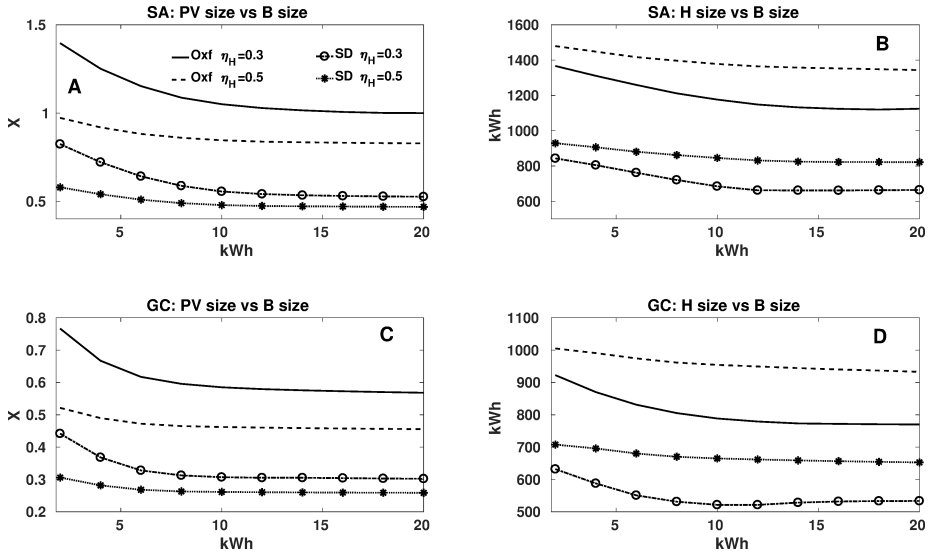

Figure 3: Panel **A**. PV array size as function of battery size in the two geolocations, for different values of hydrogen round-trip conversion efficiency. Panel **B**. Required capacity of the hydrogen reservoir as function of battery size in the two geolocations, for the same values of hydrogen conversion efficiency considered in Panel **A**. Panels **C-D** are like Panels **A-B** for the grid-connected (GC) case (Section 3.2). Legend in Panel **A** refers to all plots.

Figure 2B depicts the "roughness" parameter, defined as

$$r = \int_0^T \left| \frac{\mathrm{d}H(t)}{\mathrm{d}t} \right| \, \mathrm{d}t \,, \tag{11}$$

where continuous notation instead of discrete summation is used for generality. Roughness r helps to quantify the activity of H at small timescales typical

of battery usage: from sub-hourly to daily. Sensitivity of r to battery size, hydrogen round-trip efficiency and geolocation can be inferred from Fig. 2B: r combines the main three factors that determine the "amount of activity" of long-term storage H. Figure 2B also shows how roughness r is inversely proportional to η_H; while this result can be counterintuitive, it is physically justified because the system with more efficient long-term storage needs a smaller PV array (Fig. 1A), as a smaller amount of energy needs to be uploaded for winter months. This, in turn, implies that reliance on storage is on average higher on a daily basis; the fraction of energy "improperly" uploaded to/downloaded from the H reservoir at small timescales is consequently higher as well. Figure 4, by means of zooming on small-scale features of H's curves in Winter and Summer, provides a pictorial justification for r trends. Small batteries cause the usage of H for daily storage, as the pronounced local minima of the $B = 2$ kWh curves suggest.

3.2. Grid-connected systems

GC systems' behavior is analyzed and compared to the SA cases in two different configurations. We first postulate a grid providing a constant supply throughout the whole period, equal to 50% of the 5 MW yearly integrated load; this choice leaves to storage the burden of following demand. In the second case the given load is satisfied in both geolocations with the aid of a grid that, although still providing 50% of yearly-integrated load, is freed from the constancy constraint: power provision can oscillate randomly in time between 25% and 75% of the average demand; that is, between 143 W and 428 W.

The latter instance may exemplify a grid delivering power from intermittent sources like wind farms or solar farms: domestic storage is not only used to regularize locally generated power, but to allow the grid to deliver variable power according to instantaneous production. Similarly to what pointed out for the SA system (Section 3.1), the modeling strategy maximizes energy efficiency and therefore minimizes PV size for the given load (and for the given grid timeseries, in the random case). It will be shown in Section 5 that random permutations in hourly load produce undetectable changes in the ensuing system's size.

Figure 1B compares SA and GC systems (constant supply). An interesting conclusion is implicit in the fact that the random-supply case is virtually indistinguishable from the constant-supply one (the curve of which has therefore been omitted from the plot): the system with the 10 kWh battery is able to cope with the same effectiveness with a constant supply and with a random one. The second conclusion is that both GC systems allow a major reduction on long-term H storage in both geolocations, as neither constant not random supply suffer from PV's seasonal imbalance; however, the reduction of required H capacity is proportionally higher in Oxford, where seasonal differences in PV generation are higher. Finally, it may be worth observing the GC system in Oxford requires a PV array of the same size of the San Diego, SA system; still, the England GC system requires larger long-term storage than the California SA one.
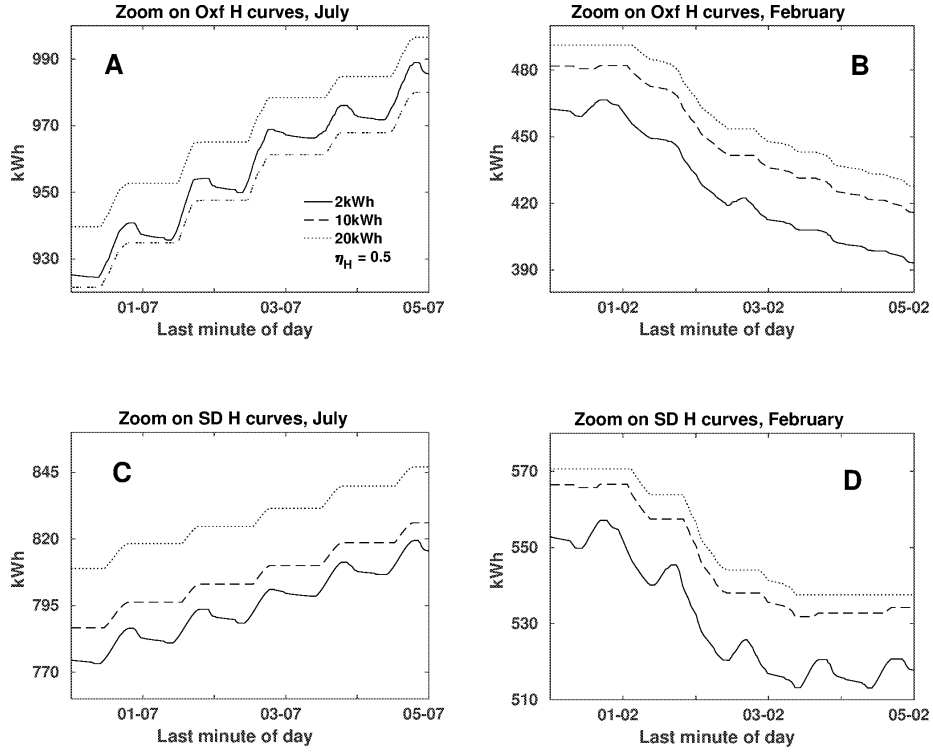
Figure 4: 5-day zooms on the curves of Fig. 2A, highlighting small-structure differences induced by battery size. A smaller B forces the system to "improperly" use long-term storage H for daily and sub-daily transactions. In Summer (Panels **A**,**C**), the curves are increasing on a sufficiently large timescale (> 1 day), as energy is being stored for the following Winter. Local minima (troughs) for the case of smallest battery (2 kWh) denote usage of H at short timescales. Larger batteries instead (dashed and dotted line) force H to follow a Summer "staircase pattern", with the hydrogen reservoir charging up in daylight and idling at nighttime. Pronounced local minima are also present in California in February in the small-battery case, because generation at that time of the year is already sufficient to store a significant amount energy from day to night. Legend in Panel **A** and H's efficiency refer to all plots. Figures B.8-B.11 in Appendix B display PV generation (bottom right Panels) for the initial two days of both 5-day periods

4. Simple CapEx analysis

The total, one-off capital cost (CapEx) of the system is examined as a function of geolocation and of H's CapEx, and in relation to the other parameters that determine system's size. The economical analysis is limited to CapEx because uncertainties on long-term storage's standards and future technical developments make detailed financial estimates difficult: for example, a gas storage tank may potentially last for an arbitrary long time while other components (fuel cells, electrolyzer) do not (Schmittinger and Vahidi, 2008; Carmo et al., 2013). This is analogous to the other systems' parts, for which expenditures are however clearer to quantify: PV systems usually require inverter replacement

at approximately the modules' midlife (Colantuono et al., 2014a), while battery duration depends on frequency and depth of discharges (Divya and Østergaard, 2009).

Even if we limit the analysis to CapEx, H's cost remains highly uncertain: neither adequate hydrogen storage facilities have been deployed so far, particularly for domestic use, nor unified technical standards exist. Economy of scale has the potential for causing a massive cost reduction, in line with what happened for decades with PV modules (International Renewable Energy Agency, 2015) and batteries (Hensley et al., 2012). Cost reduction can also be achieved by means of sharing facilities across multiple homes, which could carry the additional benefit of reducing the total required capacity. The electrolysis/fuel cells cycle is chosen in this work, but other strategies are not ruled out as H storage is here defined by round-trip efficiency, η_H, and unitary cost only. Fuel cells market price is currently around 2000 \$/kW (Crow and Johnston, 2016), while electrolyzers have been reported to be around 1000 \$/kW by Penev (2013), who also estimated the reservoir's CapEx at 2.5 \$/kW in the cheapest case (liquid hydrogen, in which case CapEx and energy expenditure for a compressor should be factored in) for large installations. 1 kW electrolyzer could suffice for coping with a load totaling 5 MWh/year; this would, however, require an extra battery to buffer the energy to be uploaded to H in instances of generation exceeding load by more than 1 kW ($\delta > 1$ kW), because B is full to capacity whenever H starts to be loaded. A similar mechanism would hold for fuel cells and the energy to be downloaded as soon as B has been depleted. The presence of such an extra battery would introduce a trade-off between its size and efficiency and fuel cells'/electrolyzer's capacities/costs, similar to the balance analyzed in this work between PV array's size/cost and battery's size/cost.

Given the large indetermination on so many factors, we let ample variation of H's CapEx , with the basic goal of determining a target range for it through the resulting CapEx of the whole system: H's CapEx is therefore allowed to vary between 0.1 \$/kWh and 70 \$/kWh. The picked cost of PV array is 3000 \$/kW$_p$ instead, while the chosen cost of batteries is 227 \$/kWh (Hensley et al., 2012).

Figures 5-6 summarize CapEx analysis. The first feature to be noticed is that, for inexpensive H, the cost curves "cluster" mainly due to B size; for expensive H, they depend more markedly on geolocation instead (Fig. 5A-B). When long-term storage is on the expensive end, H's required capacity becomes the main CapEx discriminator, meaning that the influence of geolocation on system's cost increases: Oxford's large seasonal differences in PV output require a larger amount of seasonal storage with respect to San Diego (Fig. 5A-B). The amount of long-term storage is not significantly influenced by battery size. A small battery forces the system to use seasonal storage inefficiently, on a daily/sub-daily basis (as shown by the plot of roughness r, Fig. 2B); however, the capacity used for such fast transactions is negligible ($\sim$10 kWh) and does not significantly affect the capacity involved in seasonal storage, which is of the order of 1 MWh.

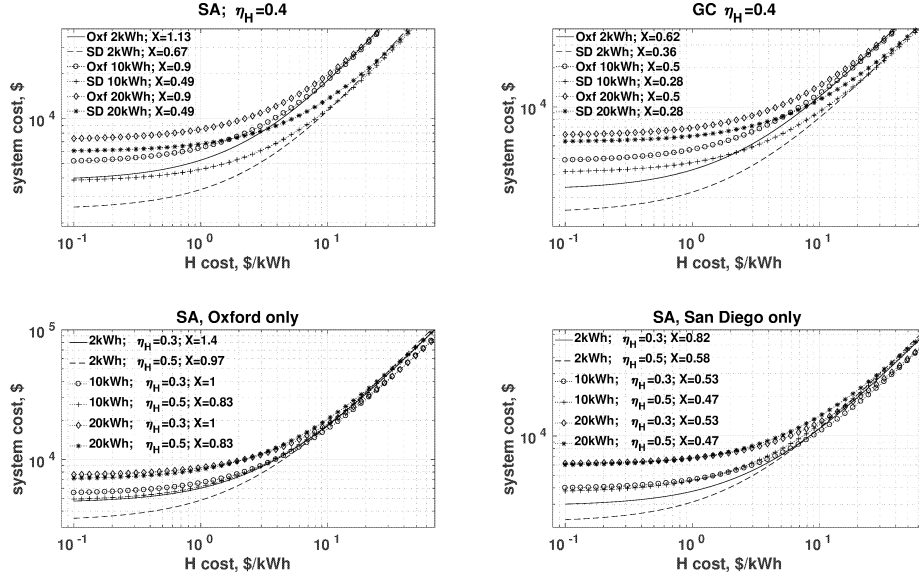Figure 5A-B show (solid curve vs dashed one) that the ratio between system

Figure 5: Summary of cost analysis. X represents the size of the PV array; $X = 1$ corresponds to an 8 kW$_{\mathrm{p}}$ array.

costs in the two geolocations does not change much as function of H cost, either with grid or without; moreover, no detectable difference exists between the case of a constant supply fed to the system and the case of a half of the integrated supply randomly varying. For negligible H's CapEx, higher Oxford's cost is due to larger PV array; as long-term storage gets more expensive and gradually becomes the main factor in determining system's cost, Oxford remains more expensive due to the much more pronounced irradiance seasonal imbalance which dictates an increase in H capacity.

Figure 5C (Oxford) and Fig. 5D (San Diego) reveal the influence of η_H on system's cost. When battery is large, a significant variation in η_H has a small impact on the system cost. With a smaller battery, on the contrary, variations in η_H are noticeable due to the increased usage of long term storage at high frequencies (daily and sub-daily) which, in turn, imposes a larger and more costly PV array. System's qualitative behavior in San Diego is very similar to Oxford in this respect, except for a generally higher cost in the more poleward location.

It may be also worth commenting on the cap that needs to be imposed on H cost in order to keep system's CapEx below a given threshold, say 10^4 \$. For SA systems, $\eta_H = 0.4$ (Fig. 5A), H's CapEx is around 4 \$/kWh in Oxford in combination with a 10 kWh battery, which increases by some tenths of \$/kWh in the same location if the battery is 2 kWh. The equivalent figures in San Diego are almost identical and higher, ~ 8 \$/kWh, because of the lower need of long-term storage capacity. Not surprisingly, the GC system receiving from the grid (Fig. 5B) 1/2 of the 5 MWh yearly integrated generation stays within

15

10^4 \$ for a higher H cost in every situation: respectively, ~ 7 \$/kWh in Oxford and more than 10 \$/kWh in San Diego for both battery sizes. A larger battery, 10 kWh or more, becomes competitive at higher systems' costs, around 2×10^4 \$ for the SA, $\eta_H = 0.4$ case (Fig. 5A). It should be kept in mind that the 2 kWh battery asks for a PV array $\sim 20\%$ larger than what needed by the 10 kWh battery; the 1.13×8 kW$_p$ array required in Oxford in the smallest battery's case (Fig.5A) corresponds to an area around 45 m^2 with current modules' conversion rate, which become more than 65 m^2 for $\eta_H = 0.3$ (Fig.5D); this figure could grow larger in case of disadvantaged PV layouts, often constrained by the built environment (Colantuono et al., 2014a). The chance of reducing PV modules' area may introduce savings or prevent additional penalties not quantified in the present calculation. This trade-off between battery capacity and PV array's area appears to be a key feature in densely populated areas with tall buildings.

As already noticed, long-term storage dominates system's CapEx when more expensive than a few \$: partly because a smaller (larger) battery requiring a larger (smaller) PV array implies these system's components partially balance each other out. The other reason is the large required capacity for seasonal storage, particularly in the poleward location. Reasonably priced long term storage appears therefore as a key condition for making SA systems viable or for allowing power grids to deliver constant or even "arbitrary" power throughout the year. As a further test, Fig. 6 reports CapEx behavior when battery cost is reduced by a factor 3, from 227 \$/kWh down to 76 \$/kWh; the larger battery becomes slightly economically convenient between 1 and 11 \$/kWh in the four cases.
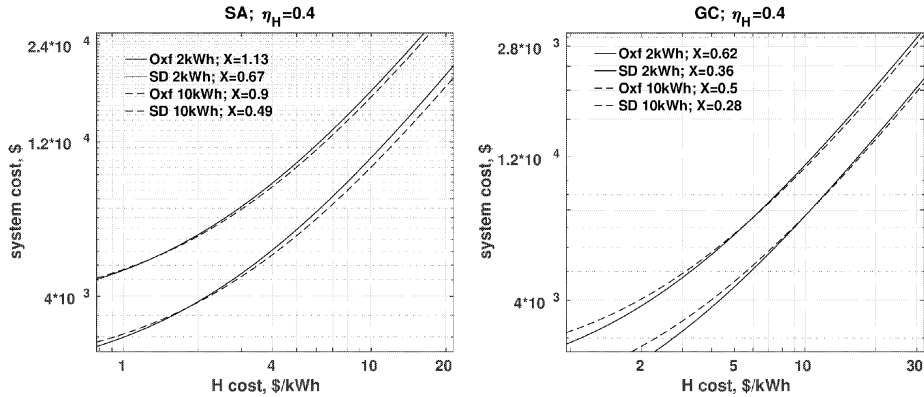

Figure 6: Like Fig. 5A-B, for B= 2kWh and B= 10kWh, and B's cost reduced by a factor 3, down to 76 \$. Both panels focus on the interval where CapEx curves for different battery sizes cross each other.

16

5. Varying demand timeseries. Extending PV generation to multiple years. Implications for system sizing

Analyzed generation and demand timeseries are 1 year-long, mainly due to data availability. In order to generalize results, we hereby show the implications of varying λ demand timeseries and considering multiple years of PV output.

λ periodicity is 60 s; in order to test sensitivity to demand's alterations, the 365×24 hours in the 1 year time interval have been randomly permuted 120 times for various parameter combinations; in all cases, the change of PV size necessary to cope with the modified load is much smaller than 1% and within the model error, which is dictated by the 10 kWh tolerance (Eq. 9) in the approximate solutions of the model equations. Similarly, the behavior of $H(t_n)$ (the graph of which is exemplified in Figs. 1 and 2A) remains practically unchanged after hours' permutations. Recalling the definition of δ (Table 1), random changes of generation γ have an effect which is similar to random variations of λ. This suggests that random generation/demand permutations do not significantly alter energy balance and system components' sizes.

Many years of PV generation need then to be considered in both geolocations, to generalize the model output and, particularly, PV array size and H's required capacity. Given the short length of the analyzed PV output, the authors turned their attention to global horizontal irradiance (GHI) timeseries spanning much longer intervals. A GHI measurement station has been chosen within 100 km of the PV location in Oxford (UK Meteorological Office 2013, station ID 461, $\sim 52.23^{\circ}$N, $\sim 0.46^{\circ}$W) and San Diego (National Solar Radiation Database 2015, station ID 210008, $\sim 32.73^{\circ}$N, $\sim 117.14^{\circ}$W); timeseries are 18 year-long (1995-2012 in Oxford; 1998-2015 in San Diego) with half-hourly/hourly (Oxford/San Diego) sampling period.

The goal is to create yearly PV generation timeseries that are, from the climate and geographical standpoint, analogous to the available ones, with 60 s sampling period. Every GHI yearly record is first normalized to the available, local yearly PV generation record. Subsequently, the local sub-hourly PV variability (obtained by subtracting the local hourly means) is linearly superimposed to the normalized GHI timeseries. Finally, the 18 yearly GHI records in each location are once more individually rescaled, this time to restore the relative, year-to-year average disparities. This way, 18 years of PV "pseudo-generation" timeseries are obtained in both locations from real GHI timeseries and used as the model input to asses the year-to-year variations in the required PV size and H's capacity (Fig. 7B,E). With the data-procedure just outlined, the reference year's record of PV generation used so far (in both Oxford and San Diego), integrated in time, constitutes by construction the average of the 18 years of pseudo-generation.

Generalizing from one to many years also sheds light on the mutual relationship between PV size X and H capacity: as Fig. 7B,E shows, such two variables are poorly correlated. An year associated to a PV array's required size larger than average is characterized by a relatively lower yearly irradiance per m^2, while a larger than average H capacity indicates reduced levels of aver-

age Winter irradiance with respect to the remainder of the year, which dictates more energy be stored in Summer. The combination of total yearly PV generation with its seasonal distribution yields the variety of cases in Fig. 7B,E. It is useful to point out that a drop in Winter generation drives a higher increase of PV size with respect to a drop of Summer yield of the same magnitude, because of the efficiency penalty affecting the energy stored from Summer to Winter. Variation of required PV size is $\sim \pm 7\%$ from average in Oxford ($\sim \pm 5\%$ in San Diego); deviations from the mean long-term storage capacity, on the contrary, are within $\sim \pm 5\%$ from average in Oxford and $\sim \pm 9\%$ in San Diego. Proportionally stronger variations of H's capacity in the latter location can be attributed to the much higher levels of Winter irradiance: even if year-to-year persistence of irradiance distribution is higher in California (as suggested by the larger variance associated to the first principal component, Fig. 7C,F), weather systems there modulate an irradiance amount that is much higher in first instance. The extension to many years suggests the order of magnitude of the sizing adjustments required to run the systems over many years, which does not reach 10% for any of the 18 years in record and for any of the systems' components.
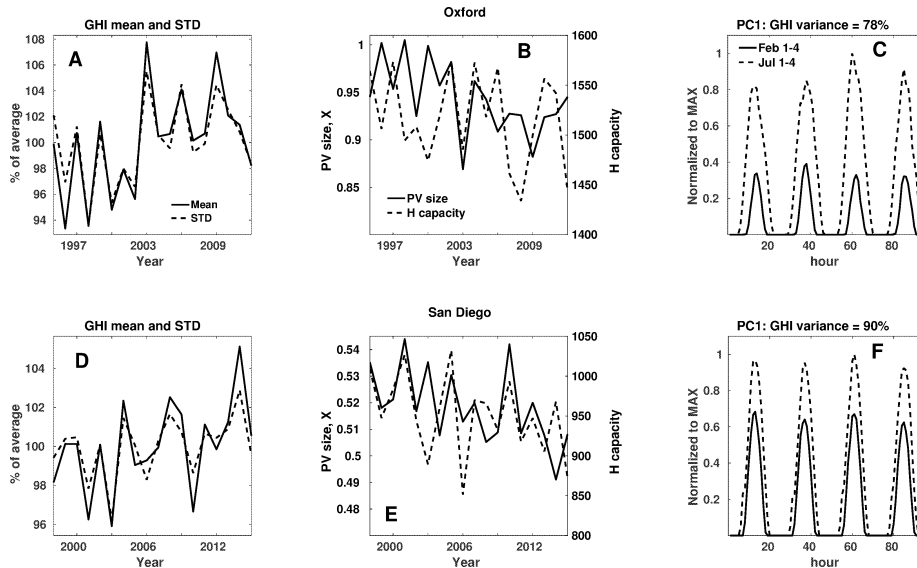
Figure 7: Panels **A,D** display GHI (kW/m^2) over the entire interval. Panels **B,E** show PV size and H capacity during 18 model runs per geolocation using PV "pseudo-generation" as input, obtained from the 18-year GHI records as described in the main text. Required storage's and PV's size variability from year to year is portrayed. In Panels **C,F** the first principal component (PC1) of the 18 yearly timeseries is plotted for a few Winter and Summer days. PC1 accounts for the day-night cycle (crests and troughs with 24 hr period) and for the seasonal cycle (greater magnitude of Summer/dashed curves' peaks with respect to solid curves' peaks). PC1 is associated to 78% of variance in Oxford and to 90% of variance in San Diego; each higher order PCs explains less than 2% of variance in Oxford (less than 1% in San Diego). The significantly higher PC1's variance in Southern California can be attributed to more stable weather with respect to the British Isles. Legend in Panel **A** refers also to Panel **D**; the same holds for Panels **B** and **E** and for **C** and **F**.

6. Discussion and Conclusions

PV arrays, combined with storage reservoirs of varying sizes, efficiencies and unitary capital costs (CapEx), are required to satisfy the same, 1-year domestic demand in two different geolocations: Oxford, England, and San Diego, California, which mutually widely differ in latitude ($\sim 20°$) and climate. The model minimizes energy use: power can be uploaded to/drawn from the least efficient reservoir (mimicking a hydrogen tank H, coupled to an electrolyzer/fuel cell cycle) only when the most efficient one (B, with an efficiency value $\eta_B = 0.85$, compatible with lithium-ion batteries' present performance) is full/empty; this rule maximizes the usage of the most efficient storage alternative. The levels of both reservoirs as function of time are output by the model; PV array size and H capacity in both locations are being sized dynamically as function of local generation per m^2, battery size and H's efficiency η_H.

The English location needs, as expected, a much larger ($\sim$170% or more, depending on parameters) PV array. It also requires an analogously larger

19

H capacity, due to the larger seasonal differences in irradiance: more energy needs to be stored during Summer months for Winter usage. Therefore, the ratio between PV sizes in Oxford and San Diego is proportionally larger than the ratio between values of yearly-integrated generation per m^2. The energy penalty (which translates into a proportionally larger PV array) imposed by a small short-term storage, with the ensuing reliance on H for short timescale storage, is proportionally higher in the equatorward location, where a significant amount of energy can be carried from day to night also during Winter.

The assumption of a standalone (SA) system is dropped and a grid introduced, which supplies 50% of the integrated yearly load. In the first case, supply is constant, meaning neither demand is followed nor grid intake can be reduced: the user is required to store the grid's provision during times of lower demand. The second case allows more freedom to the grid which, with respect to the yearly-integrated demand, supplies 25% of constant power and 25% of randomly fluctuating power. These grid-connected (GC) cases are virtually identical one to each other in terms of PV and storage sizing and of the reservoirs' state of charge. The required PV size shrinks to ∼55%-60% of the SA alone size in both geolocations.

Increasing battery size beyond ∼10 kWh does not decrease significantly either required PV size or H capacity; this holds for both SA and GC cases. 10 kWh is of the same order of magnitude of the average daily energy usage, ∼14 kWh, corresponding to 5 MWh yearly integrated value. On the contrary, a very small battery (2 kWh) requires a noticeably larger PV array, as inefficient long-term storage is "improperly" used on a daily/hourly basis. In this respect, a simple metrics has been defined to compare the behavior of the time-series representing H's charge state: the absolute value of the derivative of H's charge state, integrated over the time interval (1 year), $r = \int |\, \mathrm{d}H/\,\mathrm{d}t|\, \mathrm{d}t$, is an indicator of the amount of activity of long-term storage. High values of this quantity denote high frequency of charging-discharging cycles; low values indicate the "appropriate" use of long-term storage: bringing power from Summer to Winter. r decreases with increasing battery capacity, decreasing η_H values and decreasing latitude.

The required H capacity for B= 10 kWh and $\eta_H = 0.4$ is ∼1230 kWh in Oxford (PV array size being 93% of the local reference 8 kW$_\mathrm{p}$ system) and ∼750 kWh in San Diego (PV size 51%) for the SA system and, respectively, ∼830 kWh (PV 51%) and ∼600 kWh (28%) for GC systems.

The global minimum for PV array size is attained if the entire storage capacity is of battery type, a configuration maximizing round-trip efficiency and therefore minimizing the yearly integrated energy required to satisfy demand. It is actually the higher cost of efficient storage that suggests a multiple scale solution; a huge battery, of the order of 1 MWh, is presently not a realistic proposal for SA systems. To identify financially-plausible components' combinations, a simple cost function has been formulated. Reference costs of 3000 $/kW$_\mathrm{p}$ and 227 $/kWh are assumed for PV modules and batteries, respectively, letting H cost vary between 0.1 and 70 $/kWh. For relatively expensive H capacity (larger than 10-15 $/kWh), geolocation is the main factor to determine sys-

tem's cost; on the other hand, H costing few $ per kWh or less makes battery size as the main discriminator for total system's cost; PV's and H's sizes are inversely related and the associated expenditures partially balance out. The trade-off between PV size and battery capacity appears as a key feature of systems with long-term storage that are either standalone or partially fulfilled by a grid providing power unrelated to demand. With the specified cost for PV and batteries, a CapEx of 10^4 $ is attainable for H as expensive as 4 $/kWh in Oxford and as expensive as 8 $/kWh in San Diego (respectively 7 $/kWh and 10 $/kWh for GC systems). A large battery, with present costs of battery and PV arrays, starts to be justified in terms of CapEx for an H's cost slightly above 10 $ in all cases. Considering "cost" in a wider sense, for example factoring in the larger area taken up by the PV array required by a system endowed with a small battery, may increase the benefit of deploying a larger short-term storage capacity.

Randomly permuting hours of the demand timeseries does not affect system's sizing and behavior. Considering many years of generation causes changes in PV array's and H's capacity that are, in all conditions, less than 10% of the reference year's values. PV size variations are higher in Oxford ($\sim \pm 7\%$ vs $\sim \pm 5\%$ in San Diego), while deviations from the mean long-term storage capacity are lower there ($\sim \pm 5\%$ vs $\sim \pm 9\%$ in San Diego): higher Winter irradiance makes the equatorward location more sensitive to weather patterns than the poleward one.

6.1. Further work

Extending the analysis to diverse kinds of demand, typical of homes or businesses, will allow to understand multiple-scale storage requirements of a neighborhood or a city as a function of geolocation, with the ultimate goal of proving the feasibility of an alternative pattern for electricity distribution that does away with the load-following scheme and even with the baseload one. This will enable grids to provide power by reason of the intermittent renewables available in the region (wind farms, solar farms, etc.). Sharing batteries is likely to reduce total short-timescale capacity by averaging out individual demand patterns; similarly, sharing long-term storage between several users could provide economy of scale, but also evening out different seasonal patterns between different kind of businesses and between them and residential customers. Moreover, hydrogen used for long term storage lends itself to integration with the gas distribution network: it can be either blended with natural gas (Melaina et al., 2013), or even substitute it completely. The latter solution is being implemented in some urban areas (e.g. Leeds, UK, Sadler et al., 2016). The combination of renewables' geographical variability and multiscale storage to the energy consumption patterns of data centers is the subject of an ongoing study.

7. Acknowledgments

References

Aghaei, J. and Alizadeh, M.-I. (2013). Demand response in smart electricity grids equipped with renewable energy sources: A review. *Renewable and*

Sustainable Energy Reviews, 18:64–72.

Beaudin, M., Zareipour, H., Schellenberglabe, A., and Rosehart, W. (2010). Energy storage for mitigating the variability of renewable electricity sources: An updated review. *Energy for Sustainable Development*, 14(4):302 – 314.

Boyle, G. (2012). *Renewable electricity and the grid: the challenge of variability*. Earthscan.

Carmo, M., Fritz, D. L., Mergel, J., and Stolten, D. (2013). A comprehensive review on pem water electrolysis. *International journal of hydrogen energy*, 38(12):4901–4934.

Cau, G., Cocco, D., Petrollese, M., Kær, S. K., and Milan, C. (2014). Energy management strategy based on short-term generation scheduling for a renewable microgrid using a hydrogen storage system. *Energy Conversion and Management*, 87:820–831.

Celik, A. N. (2007). Effect of different load profiles on the loss-of-load probability of stand-alone photovoltaic systems. *Renewable Energy*, 32(12):2096–2115.

Colantuono, G., Everard, A., Hall, L. M., and Buckley, A. R. (2014a). Monitoring nationwide ensembles of pv generators: Limitations and uncertainties. the case of the uk. *Solar Energy*, 108:252 – 263.

Colantuono, G., Wang, Y., Hanna, E., and Erdélyi, R. (2014b). Signature of the north atlantic oscillation on british solar radiation availability and pv potential: The winter zonal seesaw. *Solar Energy*, 107:210–219.

Correia, J., Bastos, A., Brito, M., and Trigo, R. (2017). The influence of the main large-scale circulation patterns on wind power production in portugal. *Renewable Energy*, 102:214–223.

Crow, M. and Johnston, R. (2016). Ceres Power Holding. A fuel cell in every home and business. Technical report, Edison Investment Research Limited.

Denholm, P., O'Connell, M., Brinkman, G., and Jorgenson, J. (2015). Overgeneration from solar energy in california. a field guide to the duck chart. Technical report, National Renewable Energy Lab.(NREL), Golden, CO (United States).

Dereli, Z., Yücedağ, C., and Pearce, J. M. (2013). Simple and low-cost method of planning for tree growth and lifetime effects on solar photovoltaic systems performance. *Solar Energy*, 95:300–307.

Divya, K. and Østergaard, J. (2009). Battery energy storage technology for power systeman overview. *Electric Power Systems Research*, 79(4):511–520.

Emeis, S. (2012). *Wind energy meteorology: atmospheric physics for wind power generation*. Springer Science & Business Media.

Energy Efficiency Indicators (2016). World Energy Council. https://www.wec-indicators.enerdata.eu/household-electricity-use.html.

Erdélyi, R., Wang, Y., Guo, W., Hanna, E., and Colantuono, G. (2014). Three-dimensional solar radiation model (soram) and its application to 3-d urban planning. *Solar Energy*, 101:63–73.

Glavin, M., Chan, P. K., Armstrong, S., and Hurley, W. (2008). A stand-alone photovoltaic supercapacitor battery hybrid energy storage system. In *Power Electronics and Motion Control Conference, 2008. EPE-PEMC 2008. 13th*, pages 1688–1695. IEEE.

Hensley, R., Newman, J., and Rogers, M. (2012). Battery technology charges ahead. *McKinsey Quarterly*, 3:5–50.

International Renewable Energy Agency (2015). Renewable Power Costs Plummet: Many Sources Now Cheaper than Fossil Fuels Worldwide. Available at https://pvoutput.org/display.jsp?sid=25601.

Juul, N. (2012). Battery prices and capacity sensitivity: Electric drive vehicles. *Energy*, 47(1):403–410.

Kaplanis, S. and Kaplani, E. (2011). Energy performance and degradation over 20years performance of bp c-si pv modules. *Simulation Modelling Practice and Theory*, 19(4):1201–1211.

Klein, S. and Beckman, W. (1987). Loss-of-load probabilities for stand-alone photovoltaic systems. *Solar Energy*, 39(6):499–512.

Kleissl, J. (2013). *Solar energy forecasting and resource assessment*. Academic Press.

Lichman, M. (2013). UCI machine learning repository.

Luo, X., Wang, J., Dooner, M., and Clarke, J. (2015). Overview of current development in electrical energy storage technologies and the application potential in power system operation. *Applied Energy*, 137:511 – 536.

Mani, M. and Pillai, R. (2010). Impact of dust on solar photovoltaic (pv) performance: Research status, challenges and recommendations. *Renewable and Sustainable Energy Reviews*, 14(9):3124–3131.

Melaina, M., Antonia, O., and Penev, M. (2013). Blending Hydrogen into Natural Gas Pipeline Networks: A Review of Key Issues. https://www.nrel.gov/docs/fy13osti/51995.pdf.

Moshövel, J., Kairies, K.-P., Magnor, D., Leuthold, M., Bost, M., Gährs, S., Szczechowicz, E., Cramer, M., and Sauer, D. U. (2015). Analysis of the maximal possible grid relief from pv-peak-power impacts by using storage systems for increased self-consumption. *Applied Energy*, 137:567–575.

Mulder, G., Six, D., Claessens, B., Broes, T., Omar, N., and Van Mierlo, J. (2013). The dimensioning of pv-battery systems depending on the incentive and selling price conditions. *Applied Energy*, 111:1126–1135.

National Solar Radiation Database (2015). https://nsrdb.nrel.gov/. Accessed: 2017-07-31.

Olsson, L. E. (1994). Energy-meteorology: a new discipline. *Renewable energy*, 5(5-8):1243–1246.

Oxford PV array (2016). https://shkspr.mobi/blog/2014/12/a-year-of-solar-panels-open-data/.

Penev, M. R. (2013). Hydrogen for Energy Storage https://www.h2fcsupergen.com/wp-content/uploads/2013/06/Hybrid-Hydrogen-Energy-Storage-Michael-Penev-National-Energy-Research-Laboratory.pdf.

Prasad, A. A., Taylor, R. A., and Kay, M. (2015). Assessment of direct normal irradiance and cloud connections using satellite data over australia. *Applied Energy*, 143:301–311.

PVOutput.org (2017a). https://pvoutput.org.

PVOutput.org (2017b). https://pvoutput.org/display.jsp?sid=25601. San Diego timeseries.

PVOutput.org (2017c). https://pvoutput.org/display.jsp?sid=25687. Oxford timeseries.

Rastler, D. (2010). *Electricity energy storage technology options: a white paper primer on applications, costs and benefits*. Electric Power Research Institute.

Sadler, D. et al. (2016). h21 Leeds City Gate. https://www.northerngasnetworks.co.uk/wp-content/uploads/2017/04/h21-report-interactive-pdf-july-2016.compressed.pdf.

Schenk, K., Misra, R., Vassos, S., and Wen, W. (1984). A new method for the evaluation of expected energy generation and loss of load probability. *IEEE transactions on power apparatus and systems*, 103(2):294–303.

Schmittinger, W. and Vahidi, A. (2008). A review of the main parameters influencing long-term performance and durability of pem fuel cells. *Journal of power sources*, 180(1):1–14.

Steinke, F., Wolfrum, P., and Hoffmann, C. (2013). Grid vs. storage in a 100% renewable europe. *Renewable Energy*, 50:826–832.

UK Meteorological Office (2013). Met Office Integrated Data Archive System (MIDAS) Land and Marine Surface Stations Data (1853-current), [internet].NCAS British Atmospheric Data Centre, 2013. Available from http://badc.nerc.ac.uk/view/badc.nerc.ac.uk__ATOM__dataent_ukmo-midas.

Zhou, H., Bhattacharya, T., Tran, D., Siew, T. S. T., and Khambadkone, A. M. (2011). Composite energy storage system involving battery and ultracapacitor with dynamic energy management in microgrid applications. *IEEE transactions on power electronics*, 26(3):923–930.

Appendix A. Load and generation timeseries

The domestic electricity consumption timeseries has been downloaded from Lichman (2013). The dataset consist of about 4 years of power demand sampled every 60 s, between 2006 and 2010; year 2007 has been picked to minimize gaps. The household is located in France, is relatively substantial (includes a tumble dryer and an air conditioner) but does use gas for cooking and space heating; the latter detail is relevant as electric heating would have introduced a prominent dependency on local climate that would have made questionable the usage of such a load in an environment like San Diego, characterized by an arid climate and a significantly lower latitude.

Power generation data in Oxford has been downloaded from the web-site of a PV enthusiast who kindly makes the 2014 timeseries of his domestic system publicly available (Oxford PV array, 2016). The azimuth angle is loosely quantified as few degrees west of South, and its elevation matches the roof at apparently about 35°C. The sampling period is 60 s, as for the demand timeseries; data from the same system is also available on PVOutput.org (2017c), but with longer (300 s) sampling period. In case of gaps of 1 day or more, in this timeseries and the others, the main strategy adopted is to replace missing strings with values that are symmetrical in time with respect to the closest solstice/equinox to minimize seasonality-induced error. In case of gaps of few hours, missing strings are replaced with values from the previous/next day; gaps few minutes long have been instead filled by interpolating between nearby values. The Oxford timeseries actually runs from late December 2013 to late December 2014; the initial days of the sequence have been moved to the bottom to obtain an yearly timeseries. The size of the Oxford array is 4 kW_p; its generation is multiplied by 2 to obtain the "Oxford" load γ used here, in order to better approximate the magnitude of the demand; the ensuing 8 kW_p PV array is roughly equivalent to an area of 40 m^2, depending on technology. The precise array size that satisfies the model's equations is attained case by case and expressed by the scaling factor X.

San Diego's power generation data has been obtained from PVOutput.org (2017b); it's tilt is 22.5°C and its azimuth angle is loosely specified as "southwest". The system is larger than the Oxford one (7.8 kW_p); however, its size is not of primary interest here as its output is normalized to the Oxford, 8 kW_p array's yearly integrated generation: the ratio

$$x = \frac{\text{Oxford system yearly generation per } kW_p}{\text{San Diego system yearly generation per } kW_p} = 0.61\,, \qquad \text{(A.1)}$$

tells that an array of $0.61 \times 8 KW_p = 4.88 KW_p$ is the needed installation to achieve in San Diego the same output achieved by the $8 KW_p$ Oxford's array

for the used 1-yr timeseries. The fraction X in the main text includes this scaling factor (e.g. Fig. 1) when referred to the size of the San Diego system.

Appendix A.1. Resolution

The San Diego timeseries' sampling period is 300 s, as usual on PVOutput.org (2017a); data have been interpolated to match the 60 s-resolution of both demand (Lichman, 2013) and Oxford PV array (2016). Increasing sampling rate by interpolation could create the illusion of a battery charge state $B(t_n)$ smoother than the actual one. To bring an argument against this chance, we apply the definition of roughness (Eq. 11) to both the available Oxford PV timeseries (Oxford PV array 2016, with a 60 s sampling period, and PVOutput.org 2017c, with a 300 s period):

$$r_i = \int_0^T \left| \frac{\mathrm{d}\gamma_{O,i}(t)}{\mathrm{d}t} \right| \mathrm{d}t, \tag{A.2}$$

where γ_O represents generation in Oxford and indices denote the sampling period in seconds. We obtain

$$1 - r_{300}/r_{60} < 1\%, \tag{A.3}$$

indicating that timeseries with either 60 s or 300 s resolution produce the same model outcome in Oxford. This should be even more the case in San Diego, given the smoother behavior of irradiance in time.

Appendix B. Samples of model runs and generation

Charts in this Section display the seven variables on the left-hand sides of Eqs. (1-7) and PV generation in the SA case. Winter and Summer days are examined, with different battery sizes, to provide clues on system's behavior as parameters, geolocation and climatic conditions change. Figure B.8 shows model's variables in Oxford on two successive Winter days. On both days, generation is sufficient to upload some energy to the 4 kWh battery (as proved by the u^B panel). Due to its relatively small size, B saturates before noon (B panel) causing excess power being uploaded to H instead (u^H panel). On the second day, sunlight is weaker and the power uploaded to B is consequently smaller; the battery does not saturate and u^H is identically zero.

At the end of the 48 hour period, H's level is lower than at the beginning; power downloaded from H exceeds uploaded one, as to be expected given the season. The situation is opposite if two Summer days are considered (Fig. B.9), with H's level increased at the end of the 48 hour interval; d^H is identically zero while u^H is positive during the day, in spite of the larger battery (20 kWh) considered in this case.

In San Diego (Figs. B.10-B.11) the higher irradiance is offset by the consequently smaller size of the PV array required to meet demand; Summer-Winter imbalance is greatly reduced, like the weather modulation to the irradiance curves ("PV" subplots in Figs. B.10-B.11).
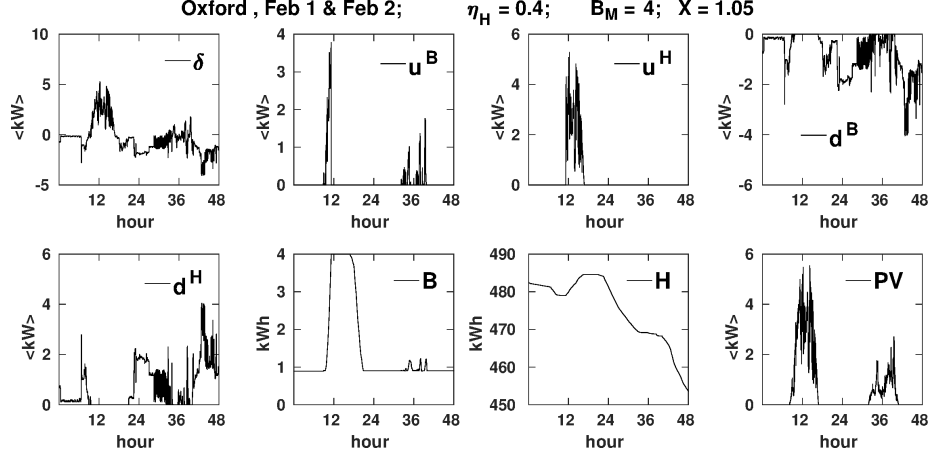
Figure B.8: System's operations are investigated in Oxford during two Winter days (reported on chart's title together with H's efficiency, battery capacity, and PV size as fraction of the reference 8 kW$_p$ array). The variables defined by Eqs. (1-7) are plotted, from left to right and top to bottom; the last (bottom-right) panel depicts PV generation. The 48 hours interval starts at 00:01 on the first day and ends at 24:00 on the second day. The <kW> label indicates power in kW averaged over every 60 s sampling interval. Power's sign is positive when uploaded to reservoirs and negative when downloaded from them. d^H, which is downloaded from H to be formally uploaded to B, is endowed with positive sign. As discussed in the main text, d^H does not undergo the energy penalty associated to battery upload in Eq. (6): even if $d^H > 0$ is indeed triggered by $B < B_m$, d^H helps meeting demand without transiting through battery.
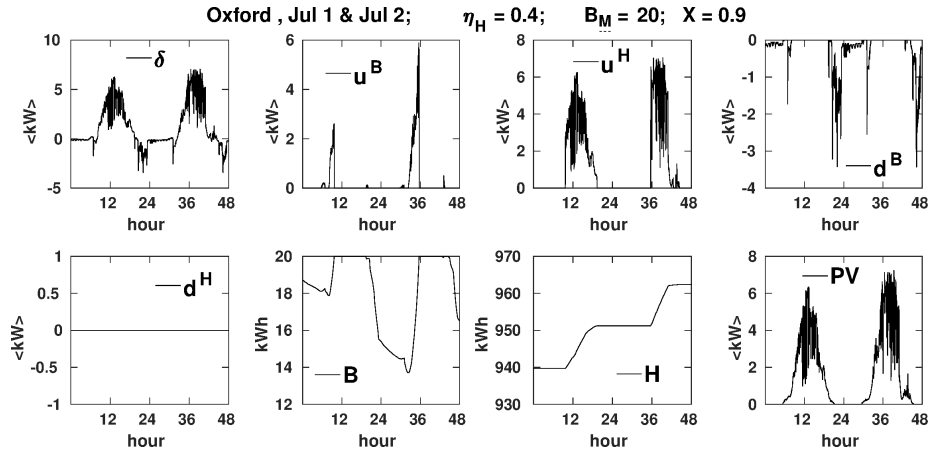

Figure B.9: Same as Fig. B.8, except that the 48 hour sampled interval belongs to July; battery capacity is 20 kWh.
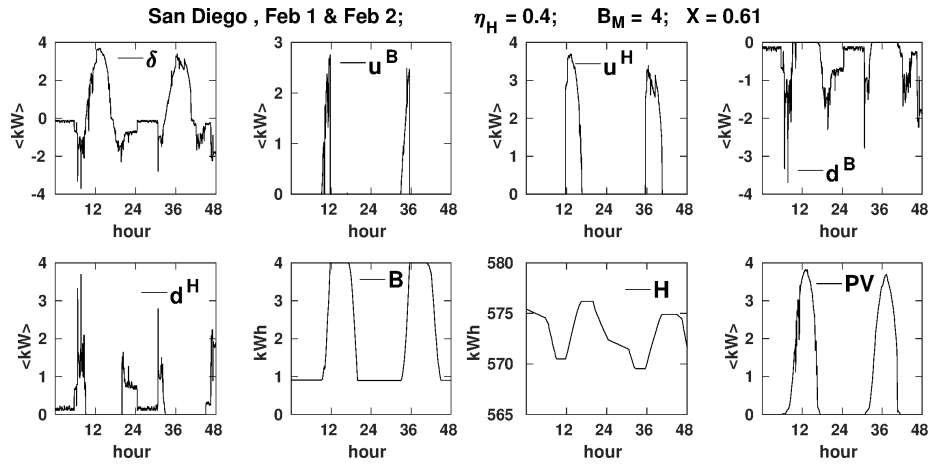
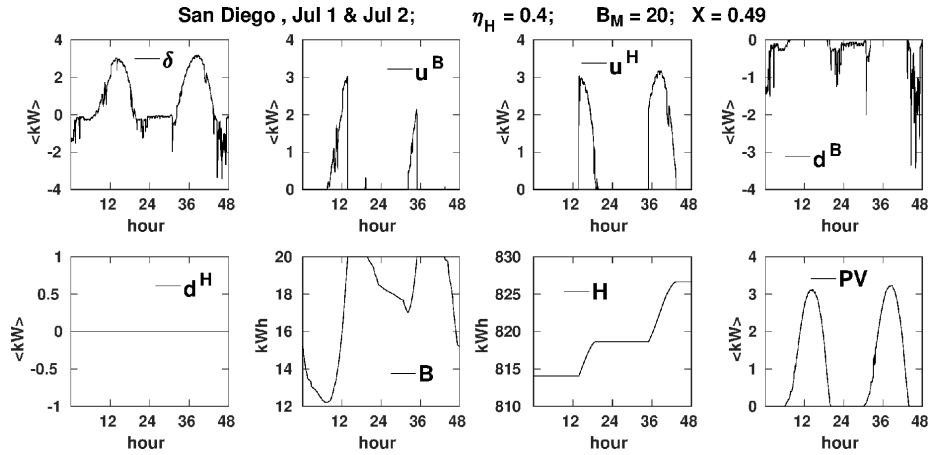Figure B.10: Equivalent to Fig. B.8 for the San Diego system.

Figure B.11: Equivalent to Fig. B.9 for the San Diego system.